Multiperipheral approach to photon-meson-Pomeron couplings

Paul M. Fishbane
Department of Physics, University of Virginia, Charlottesville, Va. 22903

Jeremiah D. Sullivan
Department of Physics, University of Illinois at Urbana-Champaign, Urbana, Illinois 61801
(Received 20 September 1977)

A multiperipheral model is used to calculate the full spin dependence of the photon-ρ-Pomeron Regge vertex function. Inclusion of both natural-parity (ω) and unnatural-parity (π) intermediate states at the top of the ladder leads to a pattern of approximate helicity conservation. The model also predicts an anomalous refractive term. The predictions of the model for the differential cross section are too small when compared to experiment, however. Photoproduction of ω, ϕ, and ψ are briefly considered as well.

I. INTRODUCTION

It is universally agreed that diffractive processes play a central role in high-energy scattering including photon-induced processes; the experimental evidence is overwhelming. In spite of this there does not yet exist a realistic, quantitative theory of diffraction scattering.

In this paper we use the multiperipheral model to make calculations of some photon-meson-Pomeron couplings. Our approach is motivated by and is a logical continuation of the now classic work of Berman and Drell[1] who used the multiperipheral model in a qualitative way to predict and describe diffractive photoproduction of vector mesons.[2]

The first part of this work is devoted to a quantitative study of the model of Berman and Drell for $\gamma N \to \rho^0 N$. We make a full calculation of the spin structure of the photon and vector-meson lines in order to compare the model to the vector-meson density-matrix elements now measured in polarized photoproduction. We find, remarkably, that when both π and ω intermediate states are included the model tends toward approximate helicity conservation for $\gamma N \to \rho^0 N$ as observed in experiments. This comes about through an approximate cancellation of π and ω (opposite parity) contributions to the helicity-nonconserving amplitudes.

The overall amplitude, however, is too small by about an order of magnitude. This is a common failure of the multiperipheral model when it is restricted to pion exchanges along the sides of the t-channel ladder. It occurs also, for example, in πN or $\pi\pi$ scattering.[3] We believe that the inclusion of higher-lying Regge trajectory exchanges may correct the normalization discrepancy without losing the tendency towards helicity conservation and the other key results which we find. Calculations of the nucleon-nucleon-Pomeron vertex have been carried out by Wingate[4] using the model developed here. He found, using only pion exchange, good agreement with experiment for both the spin dependence and the overall magnitude. We do not understand at this time why pion exchange works well for the baryon case but not the meson case.

The model used in our work is also related to that used by Kane and Pumplin[4a] in their study of the large-impact-parameter contributions to diffraction scattering. Although these authors dealt only with hadronic projectiles and did not explicitly discuss photoproduction, their findings and ours are for the most part in general agreement. One area of partial disagreement is the issue of s-channel helicity conservation. The pattern we find in ρ photoproduction and Wingate[4] finds in πN and NN scattering of a cancellation between the contributions to helicity flip amplitudes coming from natural- and unnatural-parity intermediate states is not brought out by the authors of Ref. 4(a). They point out only that specific individual intermediate state contributions do not separately conserve s-channel helicity, a result we find as well.

Care must be taken, however, to distinguish the class of diagonal and diagonal-like processes reported here and in Ref. 4 for which the phases of coupling constants are tightly constrained and the class of off-diagonal processes such as $\pi N \to A_1 N$ which were the main interest in the work of Kane and Pumplin. The relative phases of the couplings for this latter class are poorly constrained and largely unknown. Hence, approximate helicity conservation for these processes, while possible, is not compelling.

In addition to approximate helicity conservation in $\gamma N \to \rho^0 N$ we find that the model automatically incorporates in a natural way the Söding-Pumplin-Bauer mechanism[5-7] which yields the skewing of the ρ^0 mass distribution observed in experiment. Our model also predicts an anomalous "refractive" (e.g., real) part of the diffractive amplitude whose

existence was first pointed out by Bauer.[7] These topics have been discussed also by Spital and Yennie,[8] and Yennie[9] from a different but physically equivalent point of view. The anomalous real parts associated with diffractive production of unstable particles are an important feature of the Pomeranchuk contribution. We also discuss $\gamma N \to \omega N$ in the same spirit as the photoproduction of ρ^0. The prediction for the overall size of the cross section again turns out low when only pion exchange is included.

Another part of this work is devoted to a study of the photoproduction of more massive mesons. For the most part we concern ourselves with the overall size of the differential cross section, particularly at $t = 0$. One could, of course, work out the full spin structure as we have done for the ρ^0 and ω.

We take up in turn $\gamma N \to \phi N$ and $\gamma N \to \psi N$. For the latter we employ D, F, D^* and F^* intermediate mesons, charmed states which are predicted by the SU(4) model of hadrons.[10] The results differ from experimental results in the same way as our other calculations. That is, the prediction for the absolute normalization is low. However, if one considers only residue ratios the results are more successful.

II. BASIC EQUATIONS

We begin by setting down the basic multiperipheral equations and philosophy which we use throughout this paper. Figure 1 shows the multiperipheral "Pomeron" which describes the diffractive process $a + c \to a' + c$. In its original form[11,12] it was hoped that the multiperipheral ladder would be dominated by the exchange (sides of the ladder) of the lightest mass particles consistent with the quantum number constraints imposed by the external particles; normally the exchanged particles could be pions. As a result of extensive studies of the multiperipheral model it has become clear[3] that the exchange of more massive particles (ρ, ω, etc.), indeed entire Regge families, must also be included. The reason for this is the fact that these more massive mesons, while generating t-channel singularities more distant than those generated by the pion, have Regge trajectory intercepts $\alpha(0) \simeq \frac{1}{2}$ which lie above the pion intercept, $\alpha_\pi(0) \simeq 0$.

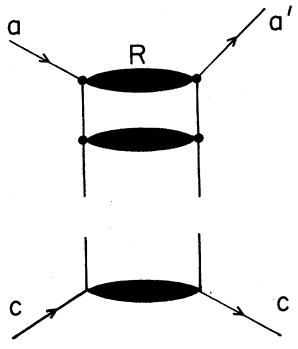

FIG. 1. Schematic representation of the multiperipheral Pomeron. The rungs of the ladder are various meson states, R. Pions (or the lightest possible particles) form the sides of the ladder.

Nevertheless, in the bulk of this paper we will restrict our discussion to the case of un-Reggeized pion exchange along the sides of the multiperipheral ladder. This is interesting because: (i) Pion exchange while not dominant is nonetheless an important component in the small t region; (ii) we are really only using pion exchange for the topmost sides of the ladder in Fig. 1 since we are only calculating the Pomeron residue functions and not the trajectory function itself; and (iii) the helicity structure and other features which we find are physically interesting in their own right and need not be obscured by details which are special to Regge exchanges.

The rungs of the multiperipheral ladder in Fig. 1 are low-mass meson states (sometimes referred to as clusters). We will make the common approximation that the rungs may be taken to be a stable hadron or a low-mass resonance. The fact that the rungs of the ladder are dominated by low-mass systems is now well established by experiment. Indeed, the study of the multiparticle final states which dominate the cross section at high energies has confirmed the basic validity of the multiperipheral approach and has begun to determine the basic input parameters.[13]

Let us first consider the case where the external particles are chosen according to $a = a'$ = pion and c = nucleon. Choosing the sides of the ladder to be pions we may pick $R = \rho(770)$ [$R = \epsilon(700)$, $f(1200)$, $g(1680)$, ... are also possible but give numerically smaller answers]. In this form the model is nothing more than an integral equation for (off shell) πN scattering as illustrated in Fig. 2.

As is well known[3] the solution of this integral equation gives a πN total cross section which falls

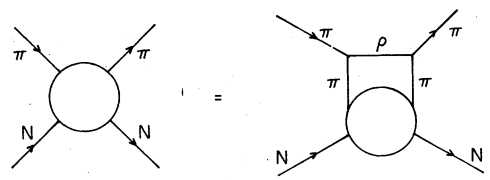

FIG. 2. Integral equation πN elastic scattering, sometimes referred to as the multiperipheral bootstrap.

with energy. In other words, the Pomeron intercept when self-consistently determined as in Fig. 2 lies below 1.

We, however, may regard Fig. 2 in a different sense. It may be interpreted as a relation between on-mass-shell πN scattering and an integral over off-mass-shell πN scattering folded with the (ρ-dominated) $\pi\pi \to \pi\pi$ amplitude. We will insert a phenomenological model for the off-mass-shell πN amplitude which has a physically correct Pomeron trajectory, $\alpha(0)=1$. The output on-mass-shell amplitude will enjoy the same correct energy dependence with a coefficient, the pion-pion-Pomeron ($\pi\pi P$) residue function, which is the object of interest. Of course we will only generate a finite fraction of this residue function since, as described above, we are restricting the uppermost (only) sides of the ladder to be pions. Before presenting numerical results for the special case of πN scattering we need to establish some notation.

For the general case $a+c \to a'+c$ we choose momenta and invariant variables as shown in Fig. 3. Namely,

$$s=(k_1+p_1)^2=(k_2+p_2)^2\equiv W^2\,, \tag{2.1a}$$

$$t=(k_1-k_2)^2=(q_1-q_2)^2=(p_1-p_2)^2\,, \tag{2.1b}$$

$$s'=(q_1+p_1)^2=(q_2+p_2)^2\,. \tag{2.1c}$$

We are interested in the leading behavior in the limit $s\to\infty$, t fixed. It is convenient to express all vectors in terms of their "plus, transverse, and minus" components[14] in the overall center-of-mass system,

$$k_1=\left(W,-\tfrac{1}{2}\vec{\Delta},\frac{\mu_1^2+\frac{1}{4}\vec{\Delta}^2}{W}\right), \tag{2.2a}$$

$$k_2=\left(W,+\tfrac{1}{2}\vec{\Delta},\frac{\mu_2^2+\frac{1}{4}\vec{\Delta}^2}{W}\right), \tag{2.2b}$$

$$p_1=\left(\frac{m_1^2+\frac{1}{4}\vec{\Delta}^2}{W},\tfrac{1}{2}\vec{\Delta},W\right), \tag{2.2c}$$

$$p_2=\left(\frac{m_2^2+\frac{1}{4}\vec{\Delta}^2}{W},-\tfrac{1}{2}\vec{\Delta},W\right), \tag{2.2d}$$

$$q_1=\left(xW,Q-\tfrac{1}{2}\vec{\Delta},\frac{\mu_1^2+\frac{1}{4}\vec{\Delta}^2}{W}-\frac{l^2+\vec{Q}^2}{(1-x)W}\right), \tag{2.2e}$$

$$q_2=\left(xW,\vec{Q}+\tfrac{1}{2}\vec{\Delta},\frac{\mu_2^2+\frac{1}{4}\vec{\Delta}}{W}-\frac{l^2+\vec{Q}^2}{(1-x)W}\right), \tag{2.2f}$$

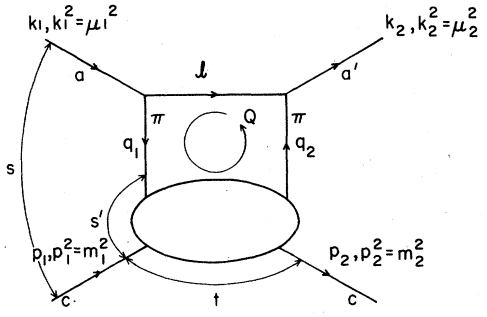

FIG. 3. Kinematics of the loop integral for the process $a+c\to a'+c$.

$$l=\left((1-x)W,-\vec{Q},\frac{l^2+\vec{Q}^2}{(1-x)W}\right). \tag{2.2g}$$

The variable x is the fraction of the large plus momentum which flows through the lines q_1 and q_2. It is useful to scale the two-dimensional transverse momenta according to

$$\vec{p}=\tfrac{1}{2}(1-x)^{1/2}\vec{\Delta}\,, \tag{2.3a}$$

$$\vec{q}=-\vec{Q}/(1-x)^{1/2}\,. \tag{2.3b}$$

Note at high energies

$$t=-\vec{\Delta}^2=-\frac{4\vec{p}^2}{(1-x)}\,, \tag{2.4}$$

$$s'=xs\,, \tag{2.5}$$

$$q_1^2=x\mu_1^2-\frac{xl^2}{(1-x)}-(\vec{p}+\vec{q})^2\,, \tag{2.6a}$$

and

$$q_2^2=x\mu_2^2-\frac{xl^2}{(1-x)}-(\vec{p}-\vec{q})^2\,. \tag{2.6b}$$

It is interesting to note that at $t=0$, (2.6a) and (2.6b) tell us that

$$q_2^2-q_1^2=x(\mu_2^2-\mu_1^2)\neq 0\,, \tag{2.7}$$

even as $s\to\infty$ when $\mu_2^2-\mu_1^2\neq 0$. Thus, processes involving large mass changes at the external lines cannot have both the internal pions simultaneously near the mass shell.

In terms of these variables the loop integration in Fig. 3 takes the form

$$M_{a'N;aN}(s,t)=\frac{1}{2}\left(\frac{i}{(2\pi)^4}\right)\int_0^1 dx\int d^2q\int dl^2\frac{g_{a\pi R}g_{a'\pi R}}{(l^2-\mu_R^2)}\frac{M_{\pi N;\pi N}(s'=xs,t;q_1^2,q_2^2)}{(q_1^2-m_\pi^2)(q_2^2-m_\pi^2)}\,, \tag{2.8}$$

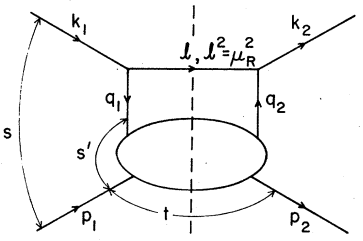

FIG. 4. The absorptive part of the graph in Fig. 3. The vertical line indicates the unitarity cut.

where M denotes the invariant amplitude. (We temporarily assume that a, a', and R are spinless.) Rather than carry out the four-dimensional integral in Eq. (2.8), it is easier to take the s-channel discontinuity of Eq. (2.8) and reduce it to a three-dimensional integration relating absoptive parts. After carrying this out Eq. (2.8) simplifies to (Fig. 4)

$$A_{a'N;aN}(s,t)=\frac{1}{2}\left(\frac{1}{(2\pi)^3}\right)\int_0^1 dx \times\int d^2q\, g_{a\pi R}g_{a'\pi R}\times\frac{A_{\pi N;\pi N}(xs,t;q_1^2,q_2^2}{(q_1^2-m_\pi^2)(q_2^2-m_\pi^2)}, \tag{2.9}$$

and in Eqs. (2.2)–(2.6) we set $l^2=\mu_R^2$. Equation (2.9) is identical to an equation derived by different techniques some time ago by Bertocchi, Fubini, and Tonin.[12]

As a phenomenological model for off-shell πN scattering we choose

$$A_{\pi N;\pi N}(s',t;q_1^2,q_2^2)=\beta e^{bt}(s'/s_0)^{\alpha(t)}\phi(q_1^2,q_2^2), \tag{2.10}$$

where $\alpha(t)$ is the Pomeron trajectory

$$\alpha(t)=1+(0.3\ \mathrm{GeV}^{-2})t, \qquad s_0=1\ \mathrm{GeV}^2, \tag{2.11}$$

and β and b are taken from experiment

$$\beta=s_0\sigma_{\mathrm{tot}}(\pi N)=64.3, \tag{2.12}$$

$$b=4.7\ \mathrm{GeV}^{-2}. \tag{2.13}$$

Note that β is the product at $t=0$ of the $\pi\pi P$ and NNP residue functions,

$$\beta=\gamma_{\pi\pi}(0)\gamma_{NN}(0). \tag{2.14}$$

All of the off-mass-shell dependence in Eq. (2.10) is contained in the factor ϕ which we assume can be represented as the product of form factors

$$\phi(q_1^2,q_2^2)=F_\pi(q_1^2)F_\pi(q_2^2), \tag{2.15}$$

whose form we discuss below. Once we have calculated $A_{a'N;aN}$ from Eq. (2.9) we can reconstruct the full amplitude from

$$M_{a'N;aN}(s,t)=A_{a'N;aN}(s,t)\left(\frac{e^{-i\pi\alpha(t)}+1}{-\sin\pi\alpha(t)}\right). \tag{2.16}$$

Substituting Eq. (2.10) into Eq. (2.9) one sees immediately

$$A_{a'N;aN}(s,t)=\left(\frac{s}{s_0}\right)^{\alpha(t)}\beta e^{bt}\tilde{\gamma}_{a'a}(t), \tag{2.17}$$

where the reduced residue function $\tilde{\gamma}_{a'a}(t)$ is given by the integral

$$\tilde{\gamma}_{a'a}(t)=\frac{1}{2}\left(\frac{1}{(2\pi)^3}\right)\int_0^1 dx\int d^2q\,\frac{g_{a\pi R}g_{a'\pi R}(x)^{\alpha(t)}}{(q_1^2-m_\pi^2)(q_2^2-m_\pi^2)}\times F_\pi(q_1^2)F_\pi(q_2^2). \tag{2.18}$$

Another feature of general interest is the phase of the scattering amplitude. For the elastic scattering of stable particles the phase is given entirely by the Regge signature factor as written in Eq. (2.16). The reduced residue functions, Eq. (2.18), are real for $t\leq 0$.

When dealing with unstable particles, however, the residue functions are not always real; this follows directly from Eq. (2.18). If during the integration over x and $\vec{q}$ one should cross the pole at $q_2^2=m_\pi^2$ (or $q_1^2=m_\pi^2$) the proper prescription is

$$\frac{1}{q_2^2-m_\pi^2}\to\frac{1}{q_2^2-m_\pi^2+i\epsilon}=\mathrm{P}\frac{1}{(q_2^2-m_\pi^2)}-i\pi\delta(q_2^2-m_\pi^2). \tag{2.19}$$

The δ-function term contributes a complex part to $\tilde{\gamma}$, and hence the overall amplitude, Eq. (2.16), picks up an *energy-independent* phase in addition to the usual signature phase. For the case of diffraction scattering at $t=0$ where the amplitude is normally pure imaginary (diffractive) the δ-function term in Eq. (2.19) contributes a real (refractive) part to the amplitude. It is easy to establish the conditions under which $\tilde{\gamma}$ becomes complex. From Eq. (2.6b), $q_2^2=m_\pi^2$ corresponds to

$$x\mu_2^2-\left(\frac{x}{1-x}\right)\mu_R^2=m_\pi^2+(\vec{p}-\vec{q})^2. \tag{2.20}$$

We may regard Eq. (2.20) as a relation among the masses. As a function of x and $\vec{q}$ the left-hand side is maximized at $x_0=1-\mu_R/\mu_2$ and the right-hand side is minimized at $\vec{p}=\vec{q}$. Hence the criterion for

a complex residue function is

$$\mu_2 \geq \mu_R + m_\pi . \tag{2.21}$$

This relation is simply the condition which states that the decay $\mu_2 \to R + m_\pi$ can physically occur, i.e., μ_2 is unstable. [Note that the signature factor prescription given in Eq. (2.16) for constructing the full amplitude from the absorptive part remains valid even when the absorptive part itself becomes complex.]

Let us now return to the πN scattering example, Fig. 2, and for simplicity specialize to $t = 0$. The product of the two coupling constants which appear in Eq. (2.18) needs only to be replaced by $\rho\pi\pi$ vertices (see Appendix A) and the ρ propagator. Namely,

$$g_{a\pi R} g_{a'\pi R} \to M_{\pi\rho\pi} = [2] g_{\rho\pi\pi}{}^2 (k_1 + q_1)\mu \left[-g^{\nu\mu} + \frac{(k_1 - q_1)^\mu (k_2 - q_2)^\nu}{m_\rho{}^2} \right] (k_2 + q_2)^\nu$$

$$= [2] g_{\rho\pi\pi}{}^2 \left[-4q_1{}^2 + \frac{1}{m_\rho{}^2} (m_\pi{}^2 - q_1{}^2 - m_\rho{}^2)^2 \right], \tag{2.22}$$

where we use $k_1 = k_2$ and $q_1 = q_2$. The overall factor of [2] in Eq. (2.22) is a Clebsch-Gordon coefficient coming from the $\rho\pi\pi$ vertices. Thus we have for the $\pi\pi P$ reduced residue function,

$$\tilde{\gamma}_{\pi\pi}(0) = [2] \left(\frac{g_{\rho\pi\pi}{}^2}{4\pi} \right) \frac{1}{(2\pi)^2} \int_0^1 dx \int d^2q x \frac{[-4q_1{}^2 - (1/m_\rho{}^2)(m_\pi{}^2 - q_1{}^2 - m_\rho{}^2)^2] F_\pi(q^2)^2}{(q_1{}^2 - m_\pi{}^2)^2} . \tag{2.23}$$

It is now necessary to specify the form factor $F_\pi(q^2)$. If we simply set $F_\pi = 1$ the transverse-momentum integration is divergent. Since the basic spirit of the multiperipheral model is a restriction to the region of low momentum transfers along the sides of the ladder we must choose F_π accordingly. The elementary divergence (which gets worse for the cases involving higher spin which we discuss below) is a signal that all results will be somewhat sensitive to the choice and scale of cutoff.

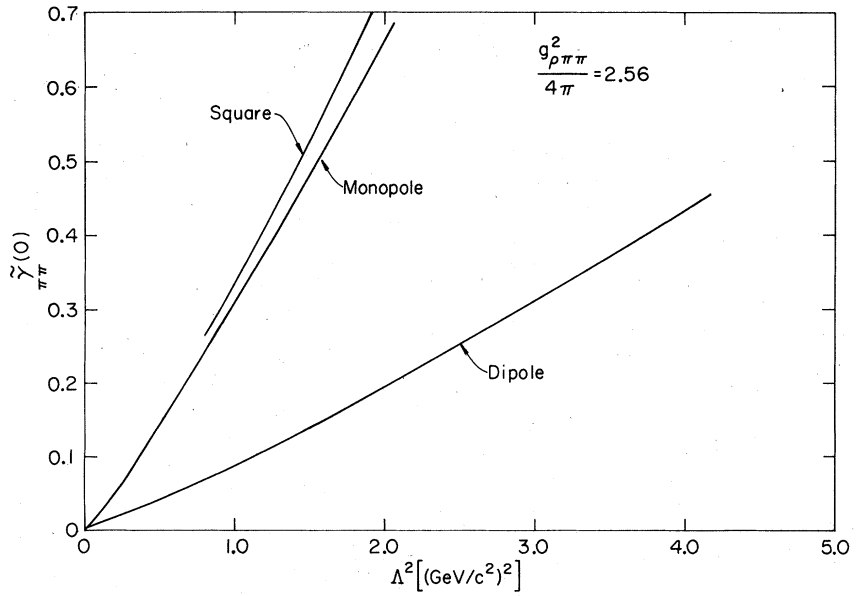

FIG. 5. Dependence of the reduced residue function, Eq. (2.23), on the cutoff mass Λ^2 in the off-shell form factor for various choices of this form factor.

We have investigated two choices:

(i) square cutoffs

$$F_\pi(q^2) = \theta(\Lambda^2 - |q^2 - m_\pi^2|) \tag{2.24}$$

and

(ii) inverse-power cutoffs

$$F_\pi(q^2) = (1 + |q^2 - m_\pi^2|/\Lambda^2)^{-N}; N = 1, 2, \ldots , \tag{2.25}$$

where Λ^2 sets the scale of the form factor. More complicated choices, e.g., exponential, Durr-Pilkuhn,[15] etc., could be made but have no special merit, at least in our case.

In Fig. 5 we illustrate the sensitivity of the quantity $\tilde{\gamma}_{\pi\pi}(0)$, Eq. (2.23), to the cutoff parameter Λ^2 for the above cutoff choices. Results were obtained by numerical integration on the computer. Note that if the simple multiperipheral model of Fig. 2 were exact, the result would be $\tilde{\gamma}_{\pi\pi}(t) = 1$ for all t. It is clear that unless Λ^2 is chosen ridiculously large $\gamma_{\pi\pi}(0)$ is about an order of magnitude too small. The methods and approximations of Ref. 4a indicate a deficiency of approximately a factor of 1/30 for this process. For definiteness we will work with a dipole form factor and $\Lambda^2 = 1.0$ GeV^2 in our subsequent work. Doubling the value of Λ^2 would roughly double the results.

III. ρ PHOTOPRODUCTION

In this section we apply the multiperipheral model, as developed in the previous section, to make detailed calculations for photoproduction of ρ^0 mesons. Extensive experimental data for the reaction exists.[16] In particular we will calculate the t dependence and the helicity dependence of the $\gamma\rho P$ residue functions as well as discuss the mechanism which causes the mass skewing in ρ photoproduction. These calculations extend the pioneering work of Berman and Drell[1] who abstracted from the multiperipheral model the key prediction that vector mesons should be produced diffractively but otherwise used it only for order-of-magnitude calculations.

In order to calculate helicity amplitudes we need explicit helicity wave functions for the incoming γ and the final ρ^0. Using the (V^+, V^x, V^y, V^-) notation of Eq. (2.2) and the same choice of coordinate system we have

$$\epsilon(\lambda_\gamma = \pm 1) = \mp \frac{1}{\sqrt{2}} \left(\frac{\sqrt{-t}}{W}, 1, \pm i, -\frac{\sqrt{-t}}{W} \right), \tag{3.1}$$

$$\epsilon(\lambda_\rho = \pm 1) = \mp \frac{1}{\sqrt{2}} \left(\frac{\sqrt{-t}}{W}, 1, \pm i, \frac{\sqrt{-t}}{W} \right), \tag{3.2a}$$

$$\epsilon(\lambda_\rho = 0) = \frac{1}{m_\rho} \left(W, \frac{\sqrt{-t}}{2}, 0, \frac{-(t/4 + m_\rho^2)}{W} \right). \tag{3.2b}$$

Note that in writing Eqs. (3.1) and (3.2) we have kept only first-order terms in the scattering angle

$$\theta \approx \frac{2\sqrt{-t}}{W},$$

which is proper in the $W \to \infty$, fixed-t limit in which we work. Since our calculations have nothing to do with the nucleon vertex it is not necessary to specify nucleon spinors or nucleon helicity indicies. In effect the nucleons may be treated as spinless.

We denote the corresponding helicity amplitudes $F_{\lambda_\rho, \lambda_\gamma}(s, t)$ by

$$\begin{aligned} F_{1,1} &= F_{-1,-1} \equiv F_1 , \\ F_{0,1} &= -F_{0,-1} \equiv F_2 , \\ F_{-1,1} &= F_{1,-1} \equiv F_3 . \end{aligned} \tag{3.3}$$

The normalization is specified by

$$\frac{d\sigma}{dt}(s, t) = \left(\frac{1}{16\pi s^2} \right) \frac{1}{2} \sum_{\lambda_\gamma} \sum_{\lambda_\rho} \left| F_{\lambda_\rho \lambda_\gamma} \right|^2 = \frac{1}{16\pi s^2} (|F_1|^2 + |F_2|^2 + |F_3|^2). \tag{3.4}$$

In addition, helicity matrix elements are defined as in Ref. 16. For our case of pure natural-parity exchange one has

$$\rho^0_{00} = |F_2|^2/D , \tag{3.5a}$$

$$\mathrm{Re}(\rho^0_{10}) = \mathrm{Re}[\tfrac{1}{2}(F_1^* - F_3^*)F_2]/D , \tag{3.5b}$$

$$\rho^0_{1,-1} = \mathrm{Re}[F_1^* F_3]/D , \tag{3.5c}$$

$$\mathrm{Im}(\rho^2_{10}) = \mathrm{Re}[\tfrac{1}{2}(A_1^* + A_3^*)A_2]/D , \tag{3.6a}$$

and

$$\mathrm{Im}(\rho^2_{1,-1}) = \tfrac{1}{2}[\,|A_3|^2 - |A_1|^2]/D , \tag{3.6b}$$

where

$$D = |F_1|^2 + |F_2|^2 + |F_3|^2 .$$

The quantities (3.5a)–(3.5c) can be measured with unpolarized photon beams. The quantities (3.6a) and (3.6b) require plane-polarized photons.

A. ω contribution

We begin with the case considered by Berman and Drell, $R = \omega(783)$, Fig. 6(a). The $\gamma\pi\omega$ and $\rho\pi\omega$

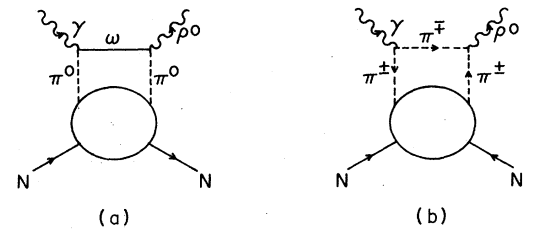

FIG. 6. The two graphs for ρ photoproduction which we consider in this paper.

vertices and couplings are specified in Appendix A. Note that they automatically satisfy gauge invariance.

The corresponding $\gamma\omega P$ residue functions are given by Eq. (2.18) after the replacement

$$g_{a\pi R}g_{a'\pi R} \to M_{\rho\omega\gamma}(\lambda_\rho, \lambda_\gamma) = \frac{g_{\gamma\pi\omega}g_{\rho\pi\omega}}{m_\omega^2}\epsilon_{\alpha\beta\gamma\delta}\epsilon^{\alpha}(k_1, \lambda_\gamma)k_1^{\beta}(k_1 - q_1)^{\delta}\left[-g^{\gamma\gamma'} + \frac{(k_1 - q_1)^{\gamma}(k_2 - q_2)^{\gamma'}}{m_\omega^2}\right]$$

$$\times\epsilon_{\alpha'\beta'\gamma'\delta'}\epsilon^{\alpha'}(k_2, \lambda_\rho)k_2^{\beta'}(k_2 - q_2)^{\delta'} . \tag{3.7}$$

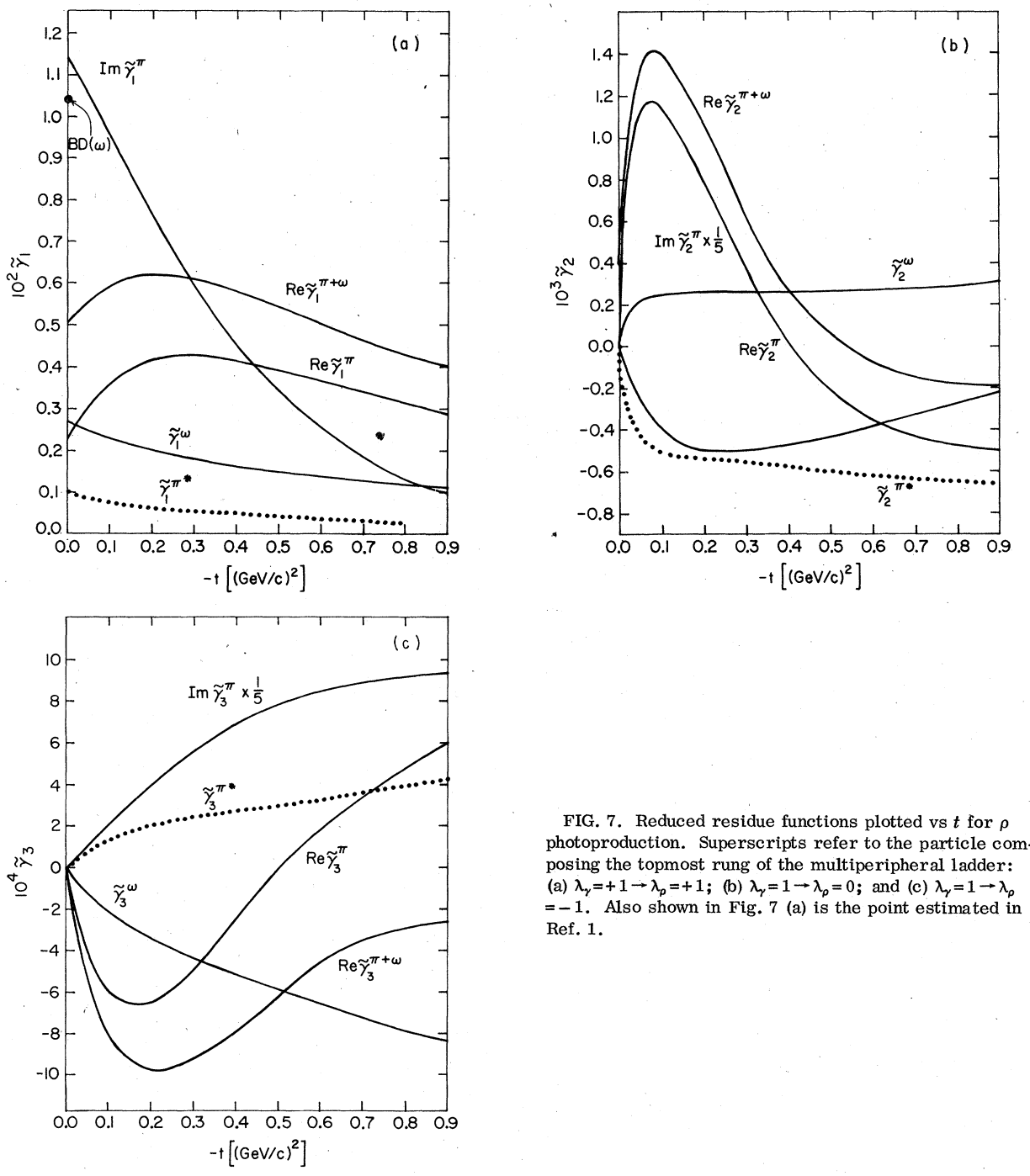

FIG. 7. Reduced residue functions plotted vs t for ρ photoproduction. Superscripts refer to the particle composing the topmost rung of the multiperipheral ladder: (a) $\lambda_\gamma = +1 \to \lambda_\rho = +1$; (b) $\lambda_\gamma = 1 \to \lambda_\rho = 0$; and (c) $\lambda_\gamma = 1 \to \lambda_\rho = -1$. Also shown in Fig. 7 (a) is the point estimated in Ref. 1.

Substituting helicity wave functions, Eqs. (3.1) and (3.2), into Eq. (3.7) we obtain the expressions for $M_{\rho\omega\gamma}(\lambda_\rho, \lambda_\gamma = 1)$, $\lambda_\rho = \pm 1$, 0 which are recorded in appendix B. Substituting these in turn into Eq. (2.18) and performing a triple numerical integration we find the reduced residue functions $\tilde{\gamma}_i^{(\omega)}(t)$. The results for a dipole form factor, cutoff $\Lambda^2 = 1.0$ $(\mathrm{GeV}/c)^2$, are shown in Figs. 7(a)–7(c). Using these one can construct the full amplitudes from Eqs. (2.16) and (2.17).

It is interesting to compare with the estimate of Berman and Drell. They worked only at $t = 0$ which means only $M_{\rho\omega\gamma}(1, 1)$ is nonzero. They assumed the integration in Eq. (2.18) was dominated by the region $q_1^2 \approx m_\pi^2$ and $x \approx 1$; effectively,

$$\frac{x}{(q_1 - m_\pi^2)} \frac{F_\pi(q_1^2)F_\pi(q_2^2)}{(q_2^2 - m_\pi^2)} \to \frac{\delta(x-1)\delta(q_1^2 - m_\pi^2)}{(q_2^2 - m_\pi^2)} \approx \frac{\delta(x-1)\delta(q_1^2)}{m_\rho^2}, \quad (3.8)$$

where the last step is obtained by using Eq. (2.7) and neglecting the pion mass squared. Hence their approximations lead to

$$\tilde{\gamma}_1^{\omega}(0) = \frac{g_{\gamma\pi\omega} g_{\rho\pi\omega}}{4\pi} \frac{1}{16\pi}. \quad (3.9)$$

This is also shown in Fig. 7(a).

B. Pion contribution

A second and important contribution to ρ photoproduction is the choice $R = \pi^\pm$, Fig. 6(b). This was not calculated by Berman and Drell in their original work. It turns out to be much more complicated than the ω intermediate state but much richer in its physical content. Numerically it is about the same size.

To calculate the π contribution to the $\gamma\rho P$ coupling we make the replacement in Eq. (2.18),

$$g_{a\pi R} g_{a'\pi R} \to M_{\rho\pi\gamma}(\lambda_\rho, \lambda_\gamma) = [2] e g_{\rho\pi\pi} \epsilon(k_1, \lambda_\gamma)^\mu (2q_1 - k_1)_\mu \epsilon(k_2, \lambda_\rho)^\nu (2q_2 - k_2)_\nu, \quad (3.10)$$

where the overall factor of [2] counts both $R = \pi^\pm$ intermediate states. If we make the replacement $\epsilon(k_1, \lambda_\gamma) \to k_1$ in Eq. (3.10) the result is nonzero except at the mass-shell point $q_1^2 = \mu^2$. Similarly, the ρ meson factor is not gauge invariant. This is a problem which frequently occurs when one-pion-exchange approximations are made in photoproduction. We cure it in a standard way, as follows:

Replace the photon coupling in Eq. (3.10) by

$$\epsilon^\mu(k_1, \lambda_\gamma)(2q_1 - k_1)_\mu \to \epsilon^\mu(k_1, \lambda_\gamma)\left[(2q_1 - k_1)_\mu - \frac{(q_1^2 - m_\pi^2)V_\mu}{k_1 \cdot V}\right], \quad (3.11)$$

where V is some four vector. The right-hand side of (3.11) is gauge invariant for any choice of V. In our work the choice $V = p_1$ is particularly attractive for two reasons. First we note that the factor of $k_1 \cdot V$ in the donominator introduces a spurious singularity into the amplitude at the point $k_1 \cdot V = 0$. The choice $V = p_1$ has the virtue that $k_1 \cdot p_1 \sim s/2$ in the limit of interest. Hence the spurious singularity is at a point far from the region in which we are applying the model and should not be serious. Second we note the additional term on the right-hand side of Eq. (3.11) is negligible compared to the first for $\lambda_\gamma = \pm 1$. It only contributes to the helicity state $\lambda_\gamma = 0$ (which is not present for real photons but possible for virtual photons).

We make a similar change in the ρ coupling except we choose $V = p_2$. Thus the final, gauge-invariant form we use in place of Eq. (3.10) is

$$M^{GI}_{\rho\pi\gamma}(\lambda_\rho, \lambda_\gamma) = [2] e g_{\rho\pi\pi} \epsilon^\mu(k_1, \lambda_\gamma)\left[(2q_1 - k_1)_\mu - \frac{(q_1 - m_\pi^2)p_{1\mu}}{p_1 \cdot k_1}\right] \epsilon^\nu(k_2, \lambda_\rho)\left[(2q_2 - k_2)_\nu - \frac{(q_2 - m_\pi^2)p_{2\nu}}{p_2 \cdot k_2}\right]. \quad (3.12)$$

Evaluating Eq. (3.12) for explicit helicity states gives the expressions recorded in Appendix B. We then use Eq. (2.18) to calculate the pion contribution to the $\gamma\rho P$ residue functions.

When carrying out the integrations we encounter the phenomenon discussed in Sec. II. Namely, because the decay $\rho \to \pi\pi$ is allowed physically, the pole at $q_2^2 = m_\pi^2$ occurs in the integration region, and the $\gamma\rho P$ residue function picks up an imaginary part. (Equivalently, the $\gamma N \to \rho N$ amplitude picks up a real part which does not vanish as $s \to \infty$.) This was first pointed out by Bauer[7] who used a different formalism but an equivalent physical approach. Note that this anomalous behavior does not occur for the ω intermediate state since $\rho \to \pi\omega$ is a closed channel.

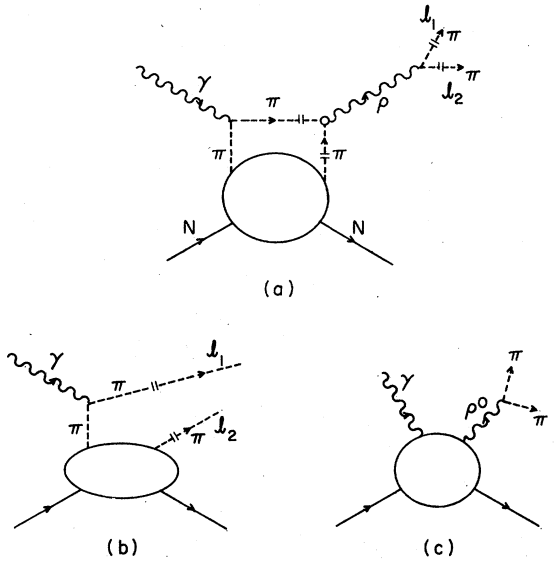

FIG. 8. Various contributions to two-pion photoproduction. Particle lines marked with a double bar are on shell. The contribution from (a), the anamalous or refractive term, is automatically included in our calculation of Fig. 6 (b). The contribution (b) is the no-scattering term and combines naturally with the result from (a). The contribution (c) is the so-called proper ρ-photoproduction amplitude. In our model this consists of Fig. 6(a) and the parts of Fig. 6(b) in which the ρ is connected by at least one off-shell pion.

This same anomalous term is intimately related to another well-known phenomenon of ρ photoproduction, the mass skewing of the ρ resonance peak. The δ-function term associated with the propagator $q_2^2 - m_\pi^2$ corresponds physically to the exchanged pion propagating on shell. The situation is illustrated in Fig. 8(a) where the double bars denote on-shell particles. We have also indicated the final decay of the ρ meson. The upper-right vertex in Fig. 8(a) where the two pions combine to form a ρ which subsequently decays back into two pions is merely a representation of $\pi - \pi$ final-state scattering. We recognize one term which is not yet included, the no scattering case, Fig. 8(b).

The contributions from Fig. 8(a) and 8(b) combine to a simple result. Namely, let $M_b(l_1, l_2)$ be the invariant amplitude (we suppress all but the pion momenta) for Fig. 8(b) and M_b^1 the piece which is a p wave in the two pions. The contribution $M_a(l_1, l_2)$ from Fig. 8(a) is, of course, pure p wave. Combining, we have

$$M_a + M_b^1 = M_b^1 \left(\frac{(m_{\pi\pi}^2 - m_\rho^2)}{(m_{\pi\pi}^2 - m_\rho^2) + i\Gamma_\rho m_\rho} \right) = M_b^1 e^{i\delta} \cos\delta , \tag{3.13}$$

where δ is the p-wave π-π scattering phase shift. Equation (3.13) was first obtained by Pumplin[6] who argued from the physical point of view that the original Söding skewing mechanism,[5] which corresponds to using M_b^1 without modification, plus the direct graph Fig. 8(c), was deficient in that it did not carry the phase of π-π elastic scattering as required by unitarity and moreover, involved some double counting. It is pleasing to see that the multiperipheral approach we are using leads in a natural and automatic way to the same conclusions. For the details of fitting the Söding-Pumplin-Bauer model to actual data we refer the reader to Refs. 8 and 16.

We finally remark that the so-called "proper" or "direct" amplitude, usually represented as in Fig. 8(c), is to be identified as the sum of all contributions to $\gamma N \to \rho^0 N$ except those where the ρ line is connected to the nucleons via two *on-the-mass-shell* pions. This is also the philosophy of Bauer.[7] Note, therefore, that contributions from our calculation of Fig. 6(b) where the ρ^0 is coupled via one (or two) *off-shell* pions are to be identified as part of the "proper" amplitude. Actually in practice this latter term should probably be split off and treated separately since it can be rapidly varying as a function of $m_{\pi\pi}$. We have calculated it only at the point $m_{\pi\pi} = m_\rho$.

Figures 7(a)–7(c) show the contribution of the pion intermediate state to the various reduced residues, including the "anomalous" imaginary part corresponding to the physical π-π state. Also shown is the sum of the ω and pion intermediate-state contributions.

To illustrate further the special features which are associated with the open channel kinematics $\rho \to \pi\pi$ we show in Figs. 7(a)–7(c) the residue functions (labeled π^*) calculated for the diagram in Fig. 6(b) where the mass of the pseudoscalar particle in the top rung is increased to m_ω. The exchanged lines remain pions with no mass change and the couplings are unchanged from the physical pion calculation.

C. Combined results and discussion

In this part we consider in detail the results from the previous subsections and make comparisons to experimental data. First consider the differential cross section.

At $t = 0$ the combined result of the π and ω intermediate-state contributions for the $s \to \infty$ asymptotic cross section for $\gamma N \to \rho^0 N$ with the coupling constants of Appendix B is

$$\left.\frac{d\sigma}{dt}\right|_{\text{proper}} = 0.77\ \mu\text{b}/(\text{GeV}/c)^2 \tag{3.14a}$$

and

$$\left.\frac{d\sigma}{dt}\right|_{\text{coherent bkg.}} = 2.5\ \mu\text{b}/(\text{GeV}/c)^2$$
$$(0.60 \leq m_{\pi\pi} \leq 0.88\ \text{GeV}). \quad (3.14b)$$

As explained above, the "proper" cross section is calculated from $\text{Re}\tilde{\gamma}^{\pi}$ and $\tilde{\gamma}^{\omega}$ whereas the coherent "background" cross section [Fig. 8(a) and 8(b)] is calculated from $\text{Im}\tilde{\gamma}^{\pi}$. These values are to be compared to the experimental value at 9.3 GeV/c (*phenomenological Söding method* of Ref. 16 adjusted to the value $\Gamma_\rho = 130$ MeV used in this paper),

$$\left(\frac{d\sigma}{dt}\right)_{\text{proper}} = (79 \pm 4)\ \mu\text{b}/(\text{GeV}/c)^2. \quad (3.15)$$

The experimental cross section decreases slightly with energy because of contributions from nonleading trajectories, but any reasonable extrapolation to high energies would give a proper forward cross section for the Pomeron contributions alone of (75 ± 5) μb/(GeV/c)^2. Thus we see that our model calculation for this piece of the *amplitude* is small by an order of magnitude.

The problem with the proper cross section is the same one we encountered in the model calculation we made in Sec. II for $\pi N \to \pi N$ scattering. There we found that the model, with reasonable choices for the form factors, gave results for $d\sigma/dt$ which were small compared to experiment by a factor ~100 (dipole form factor), ~10 (monopole form factor). (Recall $d\sigma/dt$ is proportional to the square of the quantity plotted in Fig. 5.)

In the original Berman-Drell calculation this shortfall of the model was not a problem since they worked exclusively with ratios. In effect their calculation corresponds to taking the ratio of our results in this section for $\gamma N \to \rho^0 N$ (ω only) to our results in Sec. II for $\pi N \to \pi N$. This ratio compares favorably with the corresponding experimental ratio.

One can ask at this point about the mechanisms which could bring the magnitude of the amplitude to the observed value. Among other mechanisms one could either (a) choose the cutoff mass in the form factors much larger than $\Lambda^2 = 1$ (GeV/c)^2 or (b) include other intermediate states on the top rung of the exchanged ladder (analogs to ω and π) as well as along the sides of the ladder (analogs of the π). Method (a) would scale up all the real residues in Fig. 7. The anomalous imaginary parts of the residue functions would also scale up but at a somewhat slower rate since it is only $F_\pi(q_1^2)$ which enters $[F_\pi(q_2^2 = m_\pi^2) = 1]$. Similarly, method (b) would increase the real parts of the residue functions and again have a smaller effect on the imaginary parts since $\rho \to 2\pi$ is the *only* decay channel physically open to the ρ, and hence only the subset consisting of subsititutions on the q_1 line alone will make further contributions to the anomalous piece.

Trial calculations indicate that if we increase the form-factor cutoff Λ [method (a)] the $\gamma\rho P$ residue functions $\tilde{\gamma}_i(t)$ all scale up at about the same rate. Using dipole form factors it would take, however, a value of Λ^2 in excess of 5 (GeV/c)^2 to generate the full experimental cross section in this manner (cf. Fig. 5). Such a high value for Λ^2 seems unlikely.

Since other intermediate states are certainly possible one expects some relief at least from method (b). We approach this question by imagining a spectrum of higher mass vector states in place of the ω in Fig. 6(a). As Appendix B shows, these states, like the ω, have a π-ρ vertex which requires a scale factor with the dimensions of inverse mass. The contributions of the intermediate states depend on how we treat this scale mass m_s. The most reasonable option, it seems to us, would be to take $m_s = \mu_R$, the mass of the vector intermediate state, while at the same time taking the overall dimensionless coupling constant to be the same order of magnitude as $g_{\omega\rho\pi}$. The curve (a) in Fig. 9 shows that in this scheme $d\sigma/dt$ drops very rapidly with increasing μ_R. If on the other hand we take a constant scale factor $m_s = m_\omega$ instead and keep the dimensionless coupling the same as $g_{\omega\rho\pi}$ we get the curve (b) shown in Fig. 9. In this latter

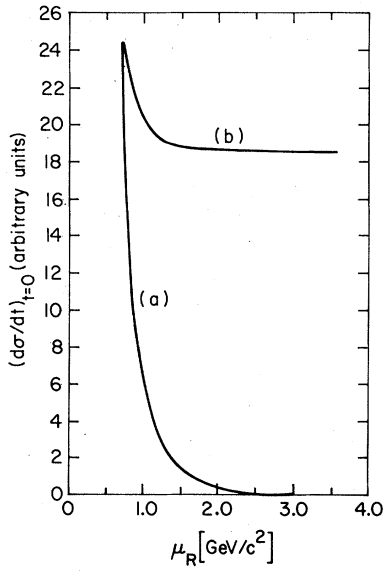

FIG. 9. The contribution of higher-mass intermediate vector states (analogous to the ω) in ρ photoproduction. Curve (a) shows the output when the scale mass in the coupling is proportional to the intermediate state mass. Curve (b) shows the output for a constant scale mass.

scheme $d\sigma/dt$ does not drop as rapidly with μ_R; nevertheless it still seems improbable that there are enough natural-parity intermediate states to build up the factor of 10 required to explain the experimental amplitude.

Similarly, consider heavier pseudoscalar intermediate states in place of the π (top rung only) in Fig. 6(b). We refer to these as π^*. Here the coupling constants are naturally dimensionless so the question of scale factor does not arise; we keep the couplings fixed. As Fig. 7(a) shows, for the case $m_{\pi^*} = m_\omega$ the contribution at $t = 0$ of such a state is only about half of the π contribution itself. [Note that π^* states do not contribute any anomalous (imaginary) part to $\tilde{\gamma}$ since the decay $\rho \to \pi\pi^*$ is energetically forbidden.] Higher values of m_{π^*} would give still smaller contributions. Again it seems unlikely that a sufficient spectrum of unnatural-parity states exists to build up the required factor of 10 in the amplitude.

Finally consider the exchange (sides of the ladder) of heavier mass *pseudoscalar* states. As the calculation of K exchange in Sec. IV shows, these contributions are similarly small. It is our belief, therefore, that the missing contributions to the amplitude come largely from replacing the pions by other meson (*Regge*) exchanges (ρ, ω, etc.) on the sides of the ladder. For an analysis of the experimental evidence from multiparticle production which indicates directly that other exchanges in addition to pion exchange are required, see Ref. 13.

As remarked above, the model predictions for the $\gamma N \to \rho^0 N$ and $\pi N \to \pi N$ amplitudes are equally low in comparison to experiment when just pion exchanges are included on the sides of the diagram in Fig. 4. We find roughly the same situation in Sec. IV for ω photoproduction. One can conjecture that this is not an accident but rather has some deeper significance. This would imply that the our model could be trusted for amplitude *ratios*.

If one adopts this point of view, consistency with the above opinion that the missing contributions to the amplitude come from Regge exchanges in place of pion exchanges in Fig. 4 implies that there is an approximate equality in the ratio of pion and individual Reggeon couplings to $\gamma\omega$ and $\pi\rho$. Namely,

$$g_{\gamma\pi\omega}/g_{\pi\pi\rho} \simeq g_{\gamma\alpha_1\omega}/g_{\pi\alpha_1\rho}\,, \tag{3.16a}$$

where the subscript α_1 denotes a Reggeon coupling.[15a] Similarly, our picture that s-channel helicity conservation comes about from cancellations between natural-parity (represented by ω) and unnatural-parity (represented by π) intermediate states is equivalent to the statement

$$g_{\gamma\pi\omega}/g_{\gamma\pi\pi} \simeq g_{\gamma\alpha_1\omega}/g_{\gamma\alpha_1\pi}\,. \tag{3.16b}$$

The question becomes, therefore, whether relations such as (3.16a) and (3.16b) are at all credible. Recalling the many approximate patterns which have been observed among Regge couplings (exchange degeneracy, f coupled Pomeron, etc.), one cannot help but speculate that further relations, such as the above, remain to be discovered. Presumably the ultimate dynamical basis for such relations resides in the fact that the π, ρ, ω, f, etc., are all built from a common quark-anti-quark pair. (We have no idea how to formulate an actual proof.) The second of the relations given above, Eq. (3.16b), seems particularly attractive if one accepts the conventional wisdom that the Reggeized multiperipheral model is a good first approximation to multiparticle production at high energy and the *experimental* fact of s-channel helicity conservation for diagonal and diagonal-like diffractive processes. Namely, as observed here and in Ref. 4(a), individual intermediate-state contributions do not conserve s-channel helicity, hence some kind of cancellation must in fact be the case. The picture that cancellation in helicity-flip amplitudes comes about trajectory by trajectory as stated by Eq. (3.16b) seems more natural than the only alternative which would have the sum of all natural-parity contributions to a given helicity-flip amplitude fortuitously cancel against the sum of all unnatural-parity contributions. Again, however, we can offer no actual proof at this time.

Next let us consider the model predictions for the density matrices. The existing experimental results (Ref. 16) for the ρ photoproduction density matrices include (unavoidably) both the "proper" and "coherent background" contributions. One must calculate the corresponding theoretical combination.

Let $F(s,t)$ be the proper amplitude and $iR(s,t)$ be the anomalous contribution calculated above at $m_{\pi\pi} = m_\rho$. The qunatities $\tilde{\gamma}_i^\omega$ and $\mathrm{Re}\tilde{\gamma}_i^\pi$ determine F; $\mathrm{Im}\tilde{\gamma}_i^\pi$ determines R. The discussion presented above showed that the full Feynman amplitude for $\gamma N \to \pi\pi N$ is

$$M(s,t,m_{\pi\pi},\theta_\pi,\phi_\pi) = \sum_\lambda \mathfrak{F}^\lambda(s,t,m_{\pi\pi}) M^\lambda(\theta_\pi,\phi_\pi)$$
$$= \left[F_\lambda\left(\frac{e^{i\delta}}{\Gamma_\rho m_\rho}\right)_{\sin\delta} + R_\lambda\left(\frac{e^{i\delta}}{\Gamma_\rho m_\rho}\right)_{\cos\delta}\right] M^\lambda\,, \tag{3.17}$$

where $M^\lambda(\theta_\pi,\phi_\pi)$ is the invariant matrix element describing the decay $\rho \to \pi^+(l_1) + \pi^-(l_2)$, λ is the helicity of the ρ, and θ_π, ϕ_π specify the direction of π^+ in the ρ rest frame. (For convenience we suppress the helicity label for the incoming photon.)

The full differential cross section is accordingly

$$d^3\sigma = \sum_\lambda \left|\mathfrak{F}^\lambda\right|^2 \frac{dt}{16\pi^2 s}\frac{dm_{\pi\pi}^2}{2\pi}(d\phi_2 |M^\lambda|^2)\,, \tag{3.18}$$

where ϕ_2 is the two-body phase space for ρ decay. Note

$$\int d\phi_2 |M^\lambda|^2 = 2m_\rho \Gamma_\rho . \tag{3.19}$$

We use Breit-Wigner forms for the phase shifts; namely,

$$e^{i\delta}\sin\delta = \frac{-m_\rho \Gamma_\rho}{m_{\pi\pi}^2 - m_\rho^2 + i m_\rho \Gamma_\rho} \tag{3.20}$$

and

$$e^{i\delta}\cos\delta = \frac{m_{\pi\pi}^2 - m_\rho^2}{m_{\pi\pi}^2 - m_\rho^2 + i m_\rho \Gamma_\rho} \tag{3.21}$$

with a constant width, $\Gamma_\rho = 130$ MeV.

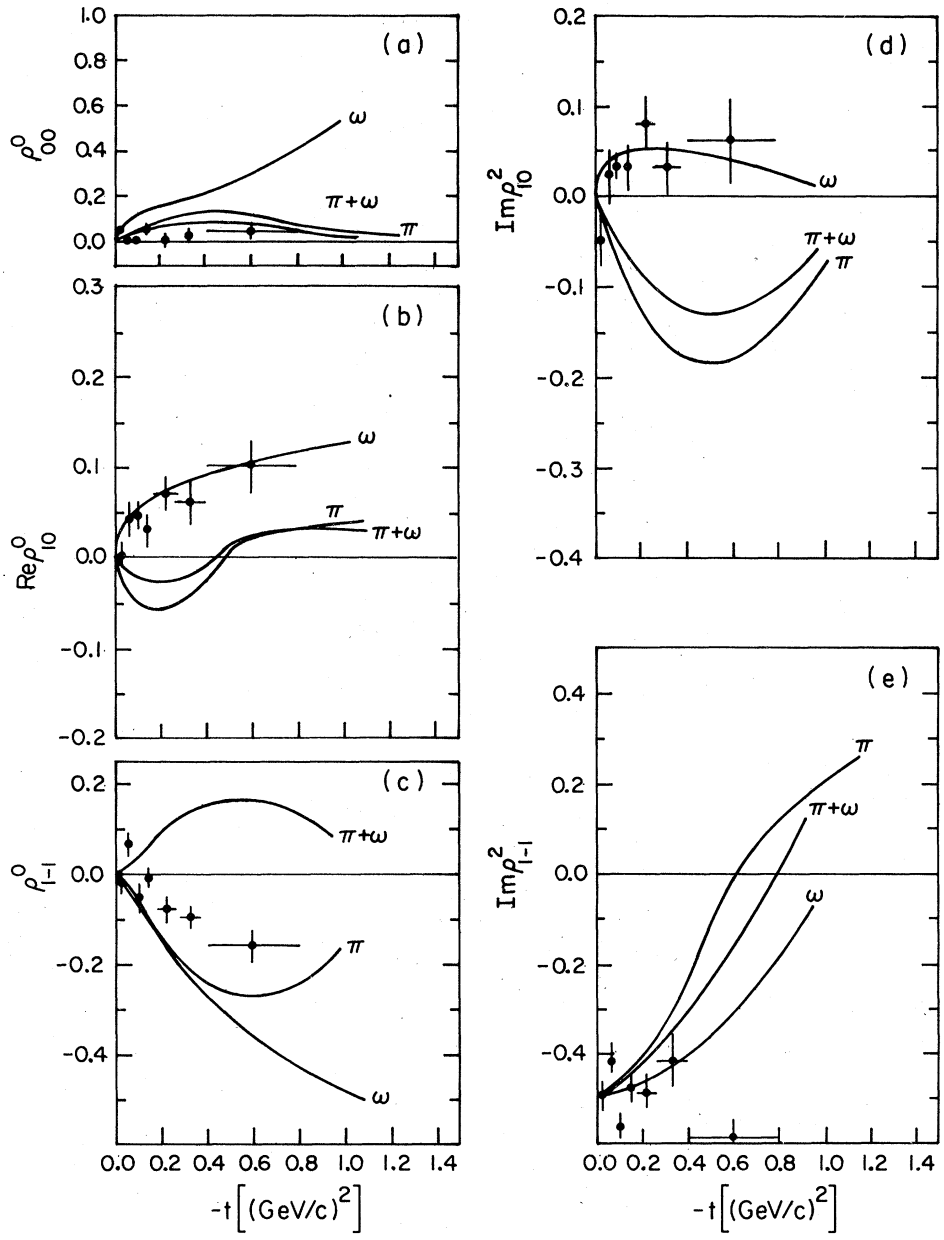

FIG. 10. Density-matrix elements as defined by Eqs. (3.5) and (3.6) in the text. The curves marked ω (π) are the predictions if only the ω (π) intermediate state is included—see Fig. 6. The curves marked $\omega+\pi$ are the predictions for the coherent sum. Note the cancellations between terms coming from π and ω intermediate states. The experimental data are from Ref. 16.

When one squares the amplitude $\mathcal{F}$ to calculate the cross section and the density-matrix elements, one encounters $\sin^2\delta$, $\cos^2\delta$, and $\sin\delta\cos\delta$ terms. The results reported in Ref. 16 correspond to the mass range $0.60 \leq m_{\pi\pi} \leq 0.88$ GeV. For this range

$$I \equiv \int dm_{\pi\pi}{}^2 \frac{\sin^2\delta}{\pi\Gamma_\rho m_\rho} = 0.71\,, \tag{3.22}$$

$$J \equiv \int dm_{\pi\pi}{}^2 \frac{\cos^2\delta}{\pi\Gamma_\rho m_\rho} = 0.61\,, \tag{3.23}$$

$$K \equiv \int dm_{\pi\pi}{}^2 \frac{\sin\delta\cos\delta}{\pi\Gamma_\rho m_\rho} = 0.06\,. \tag{3.24}$$

Thus the experiment density-matrix elements should be compared to simple generalizations of

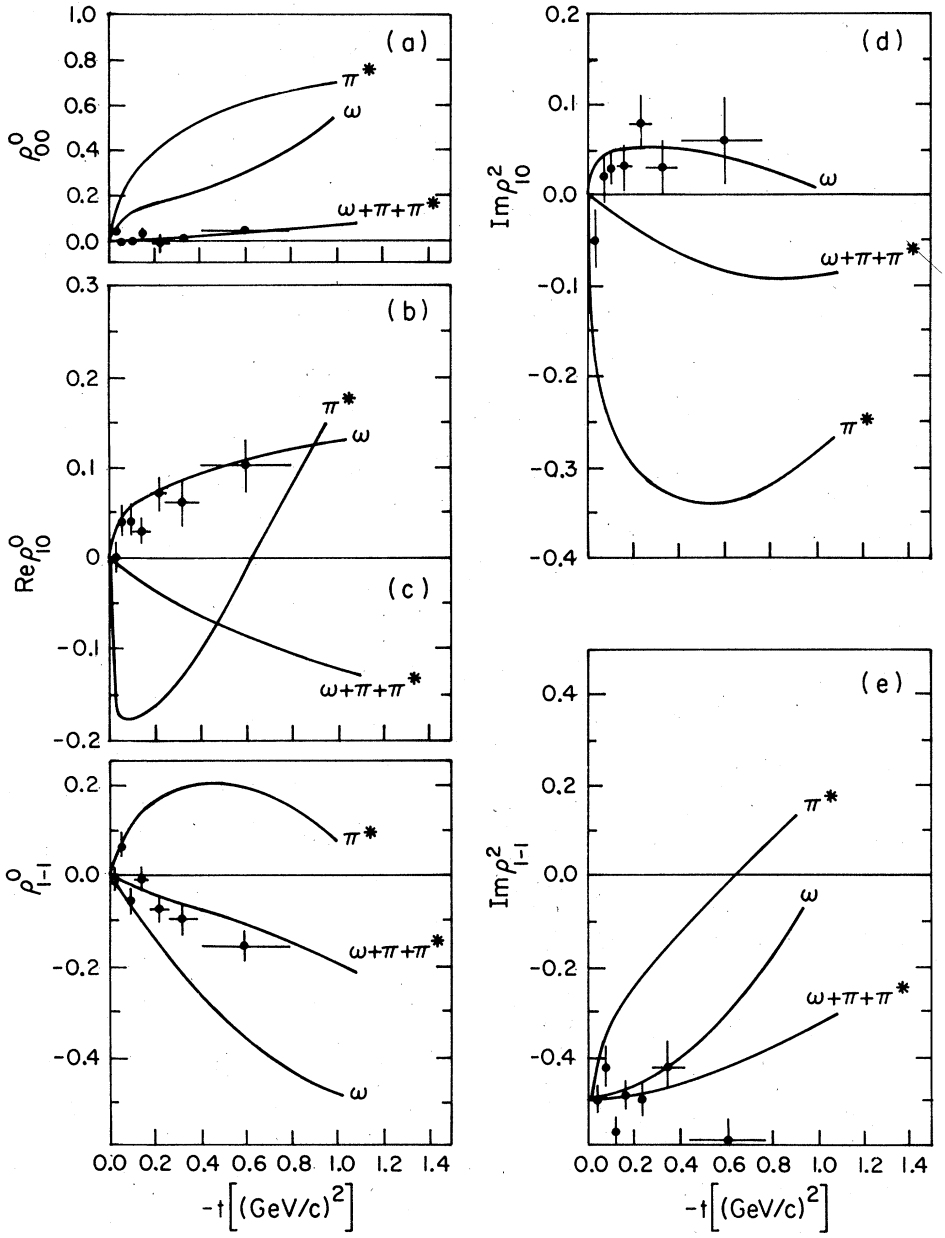

FIG. 11. Density-matrix elements as in Fig. 10 except that a heavy-mass unnatural-parity π^* contribution has been included. The theoretical predictions are those of the model after the ω and π^* amplitudes have been multiplied by 10 and the π amplitudes by 1 for the reasons discussed in the text.

Eqs. (3.5)–(3.6),

$$\rho_{00}^{0} = -\frac{(|F_2|^2 I + |R_2|^2 J + 2\,\mathrm{Re}(F_2^* R_2)K)}{\sum_{i=1}^{3}(|F_i|^2 I + |R_i|^2 J + 2\,\mathrm{Re}(F_i^* R_i)K)}, \quad (3.25)$$

and similarly for the other elements.

The model predictions are shown in Fig. 10 along with the 9.3 GeV/c data from Ref. 16. The striking feature is the substantial cancellations between the natural-parity (ω) and unnatural-parity (π) contributions in the denisty-matrix elements which correspond to $\lambda_\rho \neq \lambda_\gamma$.

Since the proper amplitude generated by our model is roughly an order of magnitude smaller than the experimentally observed proper amplitude it is difficult to draw meaningful conclusions from Fig. 10. (The coherent background is about the correct size, however.) As mentioned earlier it is quite possible that when additional contributions to the proper amplitude are found the anomalous parts will not be changed much from the values shown in Fig. 7. To illustrate the effect on the density-matrix elements we have recalculated them after multiplying the reduced residue functions $\tilde{\gamma}_i^{\omega}$ and $\tilde{\gamma}_i^{\pi *}$ in Figs. 7(a)–7(c) by 10 and the pion contributions, $\mathrm{Re}\tilde{\gamma}_i^{\pi}$ and $\mathrm{Im}\tilde{\gamma}_i^{\pi}$ by unity. The results are shown in Fig. 11. Again one sees a strong pattern of cancellation between natural-parity and unnatural-parity contributions in helicity-nonconserving terms. (This feature is also observed in Ref. 4 for the nucleon-nucleon-Pomeron vertex.) One notes that the elements involving zero helicity have the wrong sign compared to experiment. This could easily be changed by a slight variation in the enhancement factors for natural- and unnatural-parity intermediate states. However, our purpose here is only to emphasize the smallness of these elements. We believe this cancellation is general property and offers an explanation of the approximate helicity conservation observed in Pomeron dominated two-body processes.

This pattern is, of course, already evident in Figs. 7(b) and 7(c). Note that the π^* and ω helicity flip contributions have everywhere the opposite signs. It is interesting to note, however, that for $|t| \lesssim 0.5$ GeV^2 this is not the case for the π and ω contributions. This situation is another consequence of the open-channel kinematics of $\rho \to \pi\pi$. For $|t| \lesssim 0.5$ GeV^2, the dominate contribution to $\mathrm{Re}\tilde{\gamma}_{2,3}^{\pi}$ comes from integration regions in which the propagator $q_2^2 - m_\pi^2$ takes on positive (timelike) values. For larger t, negative (spacelike) values dominate. Note that $|t| \simeq 0.5$ GeV^2 is also the point at which $\mathrm{Im}\tilde{\gamma}_{2,3}^{\pi}$ cease to grow. When the top rung is π^* in place of π, $q_2^2 - m_\pi^2$ is always negative.

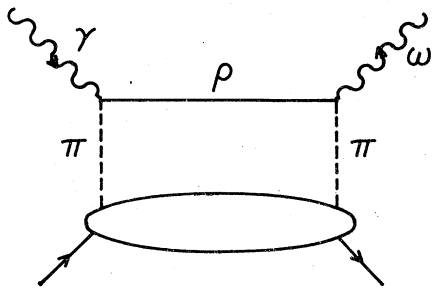

FIG. 12. The only low-mass intermediate-state contribution to ω photoproduction.

IV. ω PHOTOPRODUCTION

Figure 12 shows the diagram which is analogous to the ω intermediate state in ρ^0 photoproduction. It has an isospin weight of three compared to the corresponding amplitude for ρ^0 photoproduction. Otherwise the calculation is precisely that of ρ^0 photoproduction with a change of coupling constant. Namely,

$$\frac{d\sigma}{dt}(\gamma N \xrightarrow{\rho} \omega N) = (3)^2 \left(\frac{g_{\gamma\rho\pi}^{\ 2}}{g_{\gamma\omega\pi}^{\ 2}}\right) \frac{d\sigma}{dt}(\gamma N \xrightarrow{\omega} \rho^0 N)$$

$$= (1.2)\frac{d\sigma}{dt}(\gamma N \xrightarrow{\omega} \rho^0 N). \quad (4.1)$$

Taking the $\gamma N \xrightarrow{\omega} \rho^0 N$ amplitudes from Fig. 7 we find at $t = 0$ and ω cross section by this channel, $d\sigma/dt = 0.28\ \mu\mathrm{b}/(\mathrm{GeV}/c)^2$, compared to the high-energy experimental value[16] of ~12 μb/(GeV/c)^2, typical disagreement for the model.

The intermediate state analogous to the π in ρ^0 photoproduction would be an isospin-1, G-parity-even, pseudoscalar meson. A low-lying state with these quantum numbers does not exist, hence the density-matrix elements of ω photoproduction by the above channels will be those corresponding to the ω intermediate state in Fig. 10. Presumably higher-mass contributions would redress the balance and reestablish approximate helicity conservation.

We can also test the effect of higher-mass intermediate states as well as states on the sides of the ladder in this process. Figure 13(a) and 13(b) show

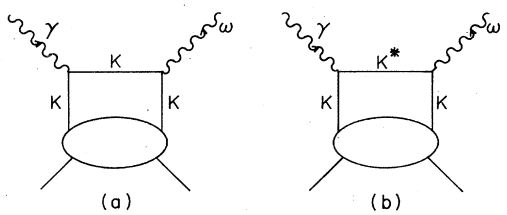

FIG. 13. Some higher-mass contributions to ω photoproduction.

two more contributions to ω photoproduction, analogous to Fig. 6(b) and 6(a), respectively. Using SU(3) values for $g_{\omega KK}$ (see Appendix A) we find, for example, that if we take the cutoff parameter as 1 GeV^2 in a dipole form factor, $d\sigma/dt\ (\gamma N \to \omega N) \simeq 0.001\ \mu\text{b}/(\text{GeV}/c)^2$. The sharp dropoff with masses of intermediate particles is typical. Computation of $\gamma N \to \omega N$ gives a similar, very small result. A more proper calculation would treat the sides of the ladder as Regge exchanges. Those with intercepts greater than zero are undoubtedly the important ones.

V. ϕ AND ψ PHOTOPRODUCTION

The case of ϕ photoproduction may present an especially interesting test because the reaction is thought to proceed *purely* by Pomeron exchange; Fig. 14 shows three contributions to ϕ photoproduction which are sizable.

We study only the size of the forward cross section here, and give the value of this quantity corresponding to the three graphs separately, rather than the coherent sum. We use values of the coupling constants given in Appendix A. Corresponding to graph (a) we find $d\sigma/dt = 2\times10^{-4}\,\mu\text{b}/(\text{GeV}/c)^2$ (a low value which results from the very small $\phi \to \pi\rho$ branching ratio); to graph (b) $d\sigma/dt = 0.03\ \mu\text{b}/(\text{GeV}/c)^2$; and to graph (c) $d\sigma/dt = 4\times10^{-6}\,\mu\text{b}/(\text{GeV}/c)^2$ (in this case the low value is associated with the large K^* mass). The major contribution thus comes from Fig. 14(b); it is the typical value of ~100 small compared to the experimental value for ϕ photoproduction[16] of $d\sigma/dt \simeq 2\ \mu\text{b}/(\text{GeV}/c)^2$.

Figure 15 shows a similar set of graphs for the photoproduction of the ψ meson. Because of the large D, D^*, F, and F^* masses, both the contributions from Figs 15(a) and (c) are strongly suppressed. Using a form factor cutoff $\Lambda^2 = 1$ (GeV/c^2)^2 as in all our previous work, $d\sigma/dt$ for Figs.

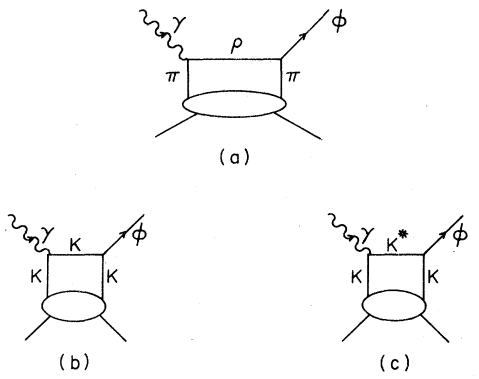

FIG. 14. Contributions to ϕ photoproduction.

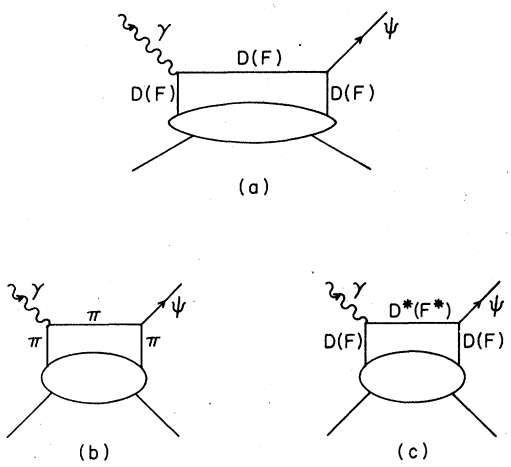

FIG. 15. Contributions to ψ photoproduction.

15(a) and 15(c) are each $\simeq 10^{-6}\ \mu\text{b}/(\text{GeV}/c)^2$. One might argue that for such states we should use a larger cutoff value. However, increasing this value to $\Lambda^2 = 4\ (\text{GeV}/c^2)^2$ increases the cross section only by a factor of $\sim 6\times10^{+3}$, entirely inadequate. Figure 15(b) is not dynamically suppressed as strongly and is dominant. However, the small $\psi \to 2\pi$ branching ratio has its effect, so that the contribution of Fig. 15(b) is $d\sigma/dt \simeq 2.5\times10^{-4}\ \mu\text{b}/(\text{GeV})^2$. One can compare this to the experimental value[17] of $50\times10^{-3}\ \mu\text{b}/(\text{GeV})^2$; again the model result is a factor of $\simeq$200 small.

VI. SUMMARY AND CONCLUSIONS

We have shown that a simple multiperipheral model of diffractive ρ photoproduction with pion exchange contains many of the features observed experimentally: approximate helicity conservation, skewing of the ρ-meson mass distribution (Söding-Pumplin-Bauer mechansim)[5-7] and an anomalous real part of the $\gamma N \to \rho N$ diffractive amplitude (Bauer effect).[7] However, as in the original work of Drell and Berman[1] the absolute normalization of the amplitude is low compared to experiment by a factor ~6–10. If one wants to retain the concept of multiperipheralism at all, the missing contributions presumably must come from multiperipheral-type diagrams where the exchanged pions are supplemented by the exchange of Regge trajectories corresponding to the vector and tensor mesons.

Generalization of the model to ω, ϕ, and ψ photoproduction show a similar shortfall of the theoretical predictions compared to experiment. Further calculations using the complete set of possible Regge exchanges in addition to the pion exchanges considered in this work would be very interesting.

ACKNOWLEDGMENT

This work was supported in part by the National Science Foundation under Grants NSF PHYS77-00151 and NSF PHYS75-21590.

APPENDIX A

In this Appendix we compile for convenience various coupling constants used in this work. A larger review is provided by Ref. 18. In some cases the couplings are directly measured (in magnitude), while in others they must be deduced from other data and theoretical input. Those couplings which can be obtained from decay widths are given in Table I without comment. We discuss the others below. In each case the choice of momentum is that indicated in Fig. 16.

The coupling $g_{\rho\pi\omega}$ can be obtained from the measured value for $g_{\gamma\pi\omega}$ by a simple vector-dominance argument[19]

$$\frac{g_{\rho\pi\omega}^2}{4\pi}=\left(\frac{f_\rho^2}{4\pi\alpha}\right)\frac{g_{\gamma\pi\omega}^2}{4\pi}=10.2\,, \tag{A1}$$

where we have used $f_\rho^2/4\pi=2.56$ from $e^+e^-\to\rho^0$ data and $g_{\gamma\pi\omega}^2/4\pi=0.029$ from the partial width for the decay $\omega\to\pi^0+\gamma$.

Recently the partial width for $\rho^-\to\pi^-+\gamma$ has been measured[20] by means of the Primakoff effect. The results of this experiment give $g_{\rho\pi\gamma}^2/4\pi=0.0013$

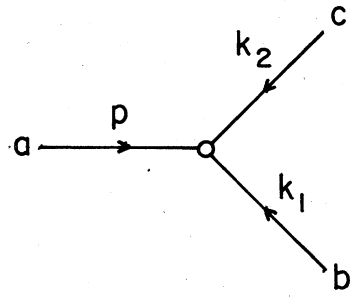

FIG. 16. Momentum and particle labelings for the calculation of coupling constants.

which, when combined with vector dominance and the value $f_\omega^2/4\pi=18.4$ from $e^-e^+\to\omega$, implies

$$g_{\rho\pi\omega}^2/4\pi=\left(\frac{f_\omega^2}{4\pi\alpha}\right)\frac{g_{\rho\pi\gamma}^2}{4\pi}=3.3\,. \tag{A2}$$

This is about a factor of three smaller than the above estimate, (A1). It is not possible to say at this time whether this indicates a substantial breakdown of vector dominance or an experimental problem.

The π^0 lifetime provides a useful consistency check. If vector dominance is assumed,[19]

$$\frac{g_{\rho\pi\omega}^2}{4\pi}=\frac{1}{2}\left(\frac{f_\rho^2}{4\pi\alpha}\right)\left(\frac{f_\omega^2}{4\pi\alpha}\right)\left(\frac{g_{\gamma\pi\gamma}^2}{4\pi}\right)=13.3\,. \tag{A3}$$

TABLE I. Definition of the vertices and numerical values for the couplings used in this work.

a	b	c	Coupling	$\Gamma_{a\to bc}$ (MeV)	$\frac{g_{abc}^2}{4\pi}$
ρ^0	$\pi^\pm$	$\pi^\mp$	$g_{\rho\pi\pi}\epsilon_\mu(p)(k_1-k_2)^\mu$	120	2.56
γ	π^0	ω	$\frac{g_{\gamma\pi\omega}}{m_\omega}\epsilon_{\mu\nu\gamma\delta}\epsilon^\mu(p)p^\nu\epsilon^\gamma(k_2)k_2^\delta$	0.87 ± 0.05	2.9×10^{-2}
$\rho^{0,\pm}$	$\pi^{0,\mp}$	γ	$\frac{g_{\rho\pi\gamma}}{m_\rho}\epsilon_{\mu\nu\gamma\delta}\epsilon^\mu(p)p^\nu\epsilon^\gamma(k_2)k_2^\delta$	0.35 ± 0.10	1.2×10^{-3} [a]
γ	π^0	γ	$\frac{g_{\gamma\pi\gamma}}{m_\rho}\epsilon_{\mu\nu\gamma\delta}k_1^\mu\epsilon^\nu(k_1)k_2^\gamma\epsilon^\delta(k_2)$	$(7.9\pm0.4)\times10^{-6}$	3.0×10^{-5}
$\rho^{0,\pm}$	$\pi^{0,\mp}$	ω	$\frac{g_{\rho\pi\omega}}{m_\omega}\epsilon_{\mu\nu\gamma\delta}\epsilon^\mu(p)p^\nu\epsilon^\gamma(k_2)k_2^\delta$	Eq. (A1) Eq. (A2) Eq. (A3)	10.2 [b] 3.3 13.3
ϕ	K^+	K^-	$g_{\phi KK}\epsilon_\mu(p)(k_1-k_2)^\mu$	1.9 ± 0.1	1.5
ϕ	$\pi^\pm$	$\rho^\mp$	$\frac{g_{\phi\rho\pi}}{m_\phi}\epsilon_{\mu\nu\gamma\delta}\epsilon^\mu(p)p^\nu\epsilon^\gamma(k_2)k_2^\delta$	0.7 ± 0.1	0.38
ψ	$\pi^\pm$	$\pi^\mp$	$g_{\psi\pi\pi}\epsilon_\mu(p)(k_1-k_2)^\mu$	2 ± 10^{-5}	0.08

[a] Not used in calculations. Instead, the vector-dominance value 4.0×10^{-3} is adopted. See text for discussion.

[b] Used in calculations.

Another estimate has been given by Renard[21] from a fit to data for the process $e^+e^- \to \omega^0 + \pi^0$. He obtains

$$\frac{g_{\rho\pi\omega}^2}{4\pi} = 23.6 . \tag{A4}$$

However, his analysis needs modification if the $\rho(1250)$ resonance suggested in Ref. 22 is confirmed.

As a working value we adopt in this paper the value of $g_{\omega\rho\pi}$ given by Eq. (A1) and listed in Table I. Moreover, we adopt the phase implied by vector-meson-dominance, namely, $g_{\gamma\pi\omega}g_{\omega\pi\rho}$ is *positive*. This assures that the amplitude for $\gamma\rho \to \rho^0 p$ has a *positive* imaginary part at high energies and $t = 0$.

Another group of coupling constants involves kaons as intermediate states. From SU(3) symmetry, we have

$$\frac{g_{\omega KK}^2}{4\pi} = \frac{1}{4}\left(\frac{g_{\rho\pi\pi}^2}{4\pi}\right) = 0.64 , \tag{A5}$$

$$\frac{g_{\omega K^*K}^2}{4\pi} = \frac{1}{4}\left(\frac{g_{\omega\rho\pi}^2}{4\pi}\right) = 2.55 , \tag{A6}$$

$$\frac{g_{\gamma KK^*}^2}{4\pi} = \frac{1}{4}\left(\frac{g_{\gamma K^0 K^{*0}}^2}{4\pi}\right) = \frac{g_{\gamma\pi\rho}^2}{4\pi} = 4.0\times 10^{-3} ,$$

$$\frac{g_{\phi K^*K}^2}{4\pi} = \frac{1}{2}\left(\frac{g_{\omega\rho\pi}^2}{4\pi}\right) = 5.1 . \tag{A7}$$

The experimental value of $g_{\gamma K^0 K^{*0}}^2$ is roughly $\frac{1}{2}$ the SU(3) value given above; the former is the value used in the text.

We also require the couplings of the ψ/J particle to the charmed mesons. SU(4) symmetry gives

$$\frac{g_{\psi FF}^2}{4\pi} = \left(\frac{g_{\psi DD}^2}{4\pi}\right) = \frac{1}{2}\left(\frac{g_{\rho\pi\pi}^2}{4\pi}\right) = 1.28 , \tag{A8}$$

$$\frac{g_{\psi F^*F}^2}{4\pi} = \left(\frac{g_{\psi D^*D}^2}{4\pi}\right) = \frac{1}{2}\left(\frac{g_{\omega\rho\pi}^2}{4\pi}\right) = 5.1 . \tag{A9}$$

Here F, D are the 0^- and F^*, D^* are the 1^- charmed mesons defined in Ref. 10.

APPENDIX B

Denote by $M_{\rho\omega\gamma}(\lambda_\rho, \lambda_\lambda)$ the numerator factors for ρ photoproduction with an $\omega(783)$ as the top rung of the multiperipheral ladder. Direct evaluation of Eq. (3.7) gives

$$M_{\rho\omega\gamma}(1,1) = \frac{g_{\gamma\pi\omega}g_{\rho\pi\omega}}{m_\omega^2}\left(-a_1 + \tfrac{1}{2}(a_2 - a_3)q^x(-zt)^{1/2} - \tfrac{1}{4}(a_2 + a_3)zt + \tfrac{1}{2}a_4 t + \tfrac{1}{2}a_5\left\{z[(q^x)^2 + (q^y)^2] + \tfrac{1}{4}z^2 t\right\}\right) , \tag{B1}$$

$$\begin{aligned} M_{\rho\omega\gamma}(1,0) = \frac{g_{\gamma\pi\omega}g_{\rho\pi\omega}}{m_\omega^2\sqrt{2}m_\rho}\Big\{ & a_1\sqrt{-t} + \tfrac{1}{4}a_2(q^x\sqrt{z} + \tfrac{1}{2}\sqrt{-t}\,z)(m_\rho^2 + t) \\ & + \tfrac{1}{2}a_3\sqrt{-t}\left[\left(m_\rho^2 + \frac{t}{4}\right)z - \frac{m_\omega^2}{z} - (q^x)^2 - (q^y)^2 + q^x(-zt)^{1/2}\right] - \tfrac{1}{2}a_4\sqrt{-t}\,(m_\rho^2 + t) \\ & - \tfrac{1}{2}a_5(q^x\sqrt{z} + \tfrac{1}{2}z\sqrt{-t})\left[\left(m_\rho^2 + \frac{t}{4}\right)z - \frac{m_\omega^2}{z} - (q^x)^2 - (q^y)^2 + q^x(-zt)^{1/2}\right]\Big\} , \end{aligned} \tag{B2}$$

and

$$M_{\rho\omega\gamma}(-1,1) = \frac{g_{\gamma\pi\omega}g_{\rho\pi\omega}}{m_\omega^2}\left(-\tfrac{1}{2}(a_2 - a_3)q^x(-zt)^{1/2} + \tfrac{1}{4}(a_2 + a_3)zt - \tfrac{1}{2}a_4 t - \tfrac{1}{2}a_5\left\{[(q^x)^2 - (q^y)^2]z + \tfrac{1}{4}z^2 t\right\}\right) , \tag{B3}$$

where $z = 1 - x$ and

$$4a_1 = 2m_\omega^2(m_\rho^2 - t) - (m_\omega^2 - q_1^2)(m_\rho^2 + m_\omega^2 - q_2^2) , \tag{B4}$$

$$4a_2 = -2(m_\rho^2 + m_\omega^2 - q_2^2) , \tag{B5}$$

$$4a_3 = -2(m_\omega^2 - q_1^2) , \tag{B6}$$

$$4a_4 = -4m_\omega^2 , \tag{B7}$$

$$4a_5 = -2(m_\rho^2 - t) . \tag{B8}$$

The numerator factors for ρ photoproduction with a pion as the top rung of the ladder as calculated from Eq. (3.12) are

$$M_{\rho\pi\gamma}^{\mathrm{GI}}(1,1) = [2]eg_{\rho\pi\pi}\left\{2[(q^x)^2 + (q^y)^2]z + \frac{t}{2}z^2\right\} , \tag{B9}$$

$$\begin{aligned} M_{\rho\pi\gamma}^{\mathrm{GI}}(0,1) = & -[2]eg_{\rho\pi\pi} \\ & \times\{m_\rho\sqrt{2z}\,(1-2x)[q^x + \tfrac{1}{2}(-tz)^{1/2}]\} , \end{aligned} \tag{B10}$$

and

$$M_{\rho\pi\gamma}^{\mathrm{GI}}(-1,1) = [2]eg_{\rho\pi\pi}\left\{-2z\left[(q^x)^2 - (q^y)^2\right] - \frac{z^2 t}{2}\right\} . \tag{B11}$$

[1]S. Berman and S. Drell, Phys. Rev. 133, B791 (1964).
[2]For other recent attempts to calculate Pomeron residues in the spirit of multiperipheralism see S. T. Jones, Phys. Rev. D 13, 1496 (1976); and J. W. Dash and S. T. Jones, *ibid.* 11, 1817 (1975). These authors were particularly interested in the t dependence of Regge residues. See also Ref. 4a.
[3]G. Chew, T. Rogers, and D. Snider, Phys. Rev. D 2, 765 (1970); M. L. Goldberger, in *Developments in High Energy Physics*, Proceedings of the International School of Physics "Enrico Fermi", Course LIV, 1971, edited by R. Gatto (Academic, New York, 1972), p. 1; D. Tow, Phys. Rev. D 2, 154 (1970).
[4]C. Wingate, Phys. Rev. D 15, 2565 (1977).
[4a]J. Pumplin and G. L. Kane, Phys. Rev. D 11, 1183 (1975).
[5]P. Söding, Phys. Rev. Lett. 19, 702 (1966). See also A. Krass, Phys. Rev. 159, 1496 (1967).
[6]J. Pumplin, Phys. Rev. D 2, 1859 (1970).
[7]T. Bauer, Phys. Rev. D 3, 2671 (1971); Phys. Rev. Lett. 25, 485 (1970); 25, 704(E) (1970).
[8]R. Spital and D. R. Yennie, Phys. Rev. D 9, 126 (1974).
[9]D. R. Yennie, Rev. Mod. Phys. 47, 311 (1975).
[10]See, e.g., M. K. Gaillard, B. W. Lee, and J. L. Rosner, Rev. Mod. Phys. 47, 277 (1975). Indeed the D and D^* have recently been discovered: G. Goldhaber, *et al.*, Phys. Rev. Lett. 37, 255 (1976).
[11]D. Amati, A. Stanghellini, and S. Fubini, Nuovo Cimento 26, 896 (1962).
[12]L. Bertocchi, S. Fubini, and M. Tonin, Nuovo Cimento 25, 626 (1962).
[13]P. Pirilä, G. Thomas, and C. Quigg, Phys. Rev. D 12, 92 (1975); S. Pinsky and G. Thomas, *ibid.* 9, 1350 (1974).
[14]These variables are defined by $p_\pm = p_0 \pm p_3$; the transverse components are untransformed. We write $p_\mu = (p_+, \vec{p}_\perp, p_-)$. These variables are closely related to the Sudakov variables. See, e.g., S. J. Chang and S.-K. Ma, Phys. Rev. 180, 1506 (1969).
[15]H. P. Dürr and H. Pilkuhn, Nuovo Cimento 40, 899 (1965).
[15a]Equations (3.16a) and (3.16b) are to be understood in a symbolic sense. Namely the coupling of a Reggeon to particles with spin will in general involve more than one coupling parameter as well as the usual nonsense factors, etc.
[16]J. Ballam *et al.*, Phys. Rev. D 5, 545 (1972); *ibid.*, 7, 3150 (1973).
[17]B. Knapp *et al.*, Phys. Rev. Lett. 34, 1040 (1975); W. Y. Lee, in *Proceedings of the 1975 International Symposium on Lepton and Photon Interactions at High Energies, Stanford, California*, edited by W. T. Kirk (Stanford Linear Accelerator Center, Stanford, 1976), p. 225.
[18]M. Nagels *et al.*, Nucl. Phys. B109, 1 (1976).
[19]M. Gell-Mann, D. H. Sharp, and W. Wagner, Phys. Rev. Lett. 8, 261 (1962).
[20]B. Gobbi *et al.*, Phys. Rev. Lett. 33, 1450 (1974).
[21]F. Renard, Nuovo Cimento 64A, 979 (1969).
[22]M. Conversi *et al.*, Phys. Lett. 52B, 493 (1974).